Influence of the Spectral Gain Suppression on the Intensities of Longitudinal Modes in 1.55 μm InGaAsP Lasers

Moustafa F. Ahmed[1], Safwat W. Z. Mahmoud[1], and Minoru Yamada[2]

[1]Department of Physics, Faculty of Science, Minia University, 61519 El-Minia, Egypt.
[2]Department of Electrical and Electronic Engineering, Faculty of Engineering, Kanazawa University, 2-40-20 Kodatsuno, Kanazawa 920-8667, Japan.

The self-suppression and both symmetric and asymmetric cross-suppressions of the gain of longitudinal modes have been analyzed in InGaAsP lasers emitting in wavelength of 1.55 μm based on a third-order perturbation approach. We compared the influences of such suppression effects of gain on the time variations of the mode intensities and the associated output spectra. Such study was based on numerical integration of the laser rate equations in a multi-mode model. Based on intensive simulations of mode dynamics, we explored the operating regions of the single- and multi-mode operations over a long scale of the strength of the asymmetric gain suppression. The results showed that the competition among the modes induces normal multimode operation under self suppression, single-mode operation in the central mode of the gain spectrum under symmetric cross-suppression, and single-mode operation with jumping of the lasing mode to the long-wavelength side of the spectrum under asymmetric gain suppression. When the asymmetric gain suppression is enhanced, transient multi-mode switching is stimulated showing asymmetric multi-mode output spectra in good correspondence with experimental results.

1. Introduction:

Fiber-To-The-Home (FTTH) networks emerge as an attractive technological target of many nations and are driving the optical communication systems into rapid developments. InGaAsP lasers emitting in wavelength of 1.55 μm are the most attractive light sources in such systems because they correspond to minimum loss as well as zero dispersion in dispersion-shifted optical fibers. When designed with Fabry-Perot (FP) cavities, these lasers are desired for low-cost subscriber networks because of their simple structure.

However, unmodulated FP-InGaAsP lasers were observed to exhibit asymmetric emission profile associated with asymmetric multi-mode output spectra [1-4]. These characteristics indicate strong gain nonlinearity of the longitudinal modes, which causes suppression of the gain of modes under the threshold gain level due to increase of their intensities [5,6].

The gain nonlinearity is caused by mode-coupling effects which originate in phase synchronization of the electric fields of modes with the electronic dipoles [5,7]. The mode coupling adds self- and cross-modal suppressing terms to the gain of each mode proportional to intensities of the modes. The influence of this type of cross-suppression is symmetric on the gain spectrum [5-7]. On the other hand, interaction of the electric fields of modes with the injected carriers may cause vibration of the carriers in the beating frequency of the modes, which contributes also to mode coupling [8-10]. Such type of coupling adds another suppressing cross-modal term to the mode gain but with asymmetric influence on the gain spectrum, that was observed in experiments [4,11]. The asymmetric gain suppression has been predicted to pronounce in lasers with a large linewidth enhancement factor such as the case of InGaAsP lasers [12,13]. Due to these mode coupling and gain nonlinearity, mode-competition phenomena are generated in the mode dynamics towards approaching the threshold gain and dominating the lasing process. Such competition is controlled by the coefficients of both the self- and symmetric and asymmetric gain suppression effects [8,9,12-14]. When the asymmetric gain suppression is weak, the mode competition is dominated by a single mode resulting in a single-mode output spectrum. Under strong asymmetric gain, the competition phenomena are enhanced stimulating complicated mode dynamics, such as temporal switching by several modes, which results in time-averaged multimode-like output spectra [12].

The aim of this paper is twofold. First we aim to present fundamental characterization of the nonlinear gain suppression effects in 1.55 μm InGaAsP lasers. For this purpose, we applied the fundamental analysis of gain suppression developed by Yamada and Suematsu based on the density-matrix approach [5]. The second aim of our work is to introduce detailed investigations of influences of the nonlinear suppression effects of gain on the mode-competition phenomena and the modal operation. The investigations were introduced in terms of time variations of the mode intensities and the associated time-averaged output spectra. The analysis in this paper is based on numerical integration of multi-mode rate equations of the modal photon numbers and the injected electron number.

This paper is structured as follows. In the next section, we present analysis of nonlinear gain in $In_xGa_{1-x}As_yP_{1-y}/InP$ lasers emitting in the wavelength of 1.55 μm. In Section 3, we introduce theoretical multi-mode

model of analysis of laser dynamics based on the characterization of gain obtained in Section 2. In Section 4, we present results of simulating the influence of nonlinear suppression effects of gain on the time variations of mode intensities and the output spectra. We also demonstrate a schematic map for regions of single- and multi-mode operations of the laser under different strengths of the asymmetric gain suppression and injection levels. Finally we conclude our work in Section 5.

2. Nonlinear gain in semiconductor lasers

2.1. Modified theory of third-order perturbation of gain

The phenomenon of gain suppression is characterized in this paper based on the third-order perturbation approach of nonlinear gain developed by Yamada and Suematsu in the density matrix analysis [5]. This approach takes into account the intraband relaxation processes of electrons which control broadening of the gain spectrum. We introduced modification to such analysis to consider transitions between the light-hole band and the conduction band in addition to the transitions from/to the heavy-hole band.

Variation of the electric field component E(r,t) in the laser cavity is described in general by the following wave equation deduced from Maxwell's equations:

$$\nabla^2 E - \mu\sigma\frac{\partial E}{\partial t} - \mu\varepsilon\frac{\partial^2 E}{\partial t^2} = \mu\frac{\partial^2 P}{\partial t^2} \tag{1}$$

where P is the electronic polarization induced due to interaction of the field with dipole moment formed by an injected electron in the conduction band and a hole in the valence band of the active region. ε and μ are the dielectric constant and magnetic permeability in the active region, respectively. In a multimode model of analysis, the electric field is expressed as,

$$E(r,t) = \sum_m \widetilde{E}_m(t)\Phi_m(r)\exp\{j\omega_m t\} + c.c. \tag{2}$$

where $\widetilde{E}_m(t)$ is a slowly time-varying amplitude of the field of mode $m = 0,\pm1,\pm2,....,\pm M$ that vibrates in an angular frequency ω_m. $\Phi_m(r)$ is the mode spatial distribution function and is characterized inside the laser cavity by:

$$\left(\nabla^2 + \omega_m^2\mu\varepsilon\right)\Phi_m(r) = 0 \tag{3}$$

$$\int_{laser} \left|\Phi_m(r)\right|^2 d^3r = 1 \tag{4}$$

By substituting the filed expression (2) as a solution of Eq. (1) assuming harmonic time-rotation of P, the following equation for time evolution of the field intensity $\left|\widetilde{E}_m(t)\right|^2$ is obtained:

$$\frac{d}{dt}\left|\widetilde{E}_m\right|^2 = \frac{c}{n_r}\left[g_m - g_{th}\right]\left|\widetilde{E}_m\right|^2 + C_m \tag{5}$$

where g_m is the gain of mode m and is calculated in terms of the induced polarization P as,

$$g_m = \frac{\omega_m}{cn_r}\frac{1}{\Delta t}\,\mathrm{Im}\left\{\int_{\mathrm{V}}\int_{t}^{t+\Delta t}\frac{P}{\widetilde{E}_m}\Phi_m^*(r)\exp\{-j\omega_m t\}\,dt\,dr\right\} \tag{6}$$

The time interval $\Delta t\left(\approx 1/\omega_m\right)$ is introduced to obtain the time-averaged value with respect to the optical frequency. c is the speed of light in vacuum and n_r is the refractive index in the active region whose length is L and volume is V. In Eq. (5), g_{th} is the threshold level of gain and C_m is the contribution of the spontaneous emission into the resonant mode m.

The polarization P is calculated quantum mechanically as the expectation value of the dipole moment operator R [5]. Due to mathematical complexity of the analysis, a closed form can not be derived for P unless several approximations are followed, such as homogenous broadening of gain and a plane-wave picture of the field [7,15]. Alternatively, P has been calculated by applying perturbation approaches in terms of the electric field in the statistical density matrix analysis [5-7,15]. The modal gain g_m is then given by the expansion,

$$g_m = g_m^{(1)} - \sum_n g_{m(n)}^{(3)}\left|\overline{E}_n\right|^2 + \ldots\ldots \tag{7}$$

where the even-order terms vanish due to the off-diagonal nature of the dipole moment operator. It has been proved that the contributions of the expansion terms of gain higher than the third order are negligible and can be ignored within the normal operation of lasers [15]. The first- and third-order gain coefficients are calculated by the following equations [5]:

$$g_m^{(1)} = \int_V g^{(1)}\left|\Phi_m(\mathrm{r})\right|^2 \mathrm{d}^3\mathrm{r} \tag{8}$$

$$g_{m(n)}^{(3)} = \int_{V} g^{(3)} \left|\Phi_m(r)\right|^2 \left|\Phi_n(r)\right|^2 \, \mathrm{d}^3\mathrm{r} \qquad (9)$$

where $g^{(1)}$ and $g^{(3)}$ are material gain coefficients independent of the laser geometry. The forms of these coefficients given in [4] are modified to:

$$g^{(1)} = \frac{\omega_m}{c\varepsilon_0 n_r \tau_{in} \hbar} \sum_{j=h,\ell} \int_{E_g}^{\infty} \left|R_{ab}\right|^2 \frac{g_{cvj}\left[f_{cj}(\hbar\omega_{ba}) - f_{vj}(\hbar\omega_{ba})\right]}{(\omega_m - \omega_{ba})^2 + (1/\tau_{in})^2} d(\hbar\omega_{ba}) \qquad (10)$$

$$g^{(3)} = \frac{\omega_m}{c\varepsilon_0 n_r \tau_{in} \hbar^3} \sum_{j=h,\ell} \int_{E_g}^{\infty} \left|R_{ab}\right|^2 g_{cvj}\left[f_{cj}(\hbar\omega_{ba}) - f_{vj}(\hbar\omega_{ba})\right] \mathrm{Re}\left\{\left[\frac{2(\tau_c + \tau_v)/\tau_{in}}{(\omega_m - \omega_{ba})^2 + (1/\tau_{in})^2}\right.\right.$$

$$\left.\left. + \left(\frac{1}{j(\omega_m - \omega_{ba}) + 1/\tau_{in}} + \frac{1}{j(\omega_{ba} - \omega_n) + 1/\tau_{in}}\right)\left(\frac{1}{j(\omega_m - \omega_n) + 1/\tau_c} + \frac{1}{j(\omega_m - \omega_n) + 1/\tau_v}\right)\right]\right.$$

$$\left. \mathrm{X} \frac{1}{j(\omega_m - \omega_{ba}) + 1/\tau_{in}}\right\}(\hbar\omega_{ba}) \qquad (11)$$

where $\hbar\omega_{ba} = \hbar\omega_b - \hbar\omega_a$ is the energy difference between level *b* in the conduction band and level *a* in the valence band. The summation in the above equations are to take into account the electron transitions between the light-hole band ($j=\ell$) and heavy-hole band ($j=h$) and the conduction band. The functions $f_{cj}(\hbar\omega_{ba})$ and $f_{vj}(\hbar\omega_{ba})$ are Fermi-Dirac distribution functions in the conduction and valence bands, respectively and $g_{cvj}(\hbar\omega_{ba})$ is the joint density of states. These functions are determined by the quasi-Fermi levels μ_c and μ_v in the conduction and valence bands, respectively as well as the effective mass at the conduction band m_c and the effective masses at the light-hole and heavy-hole bands m_{vl} and m_{vh}, respectively. Forms of these functions can be found in [16]. Dependence of the dipole moment R_{ab} on the photon energy is described by the equation [17]:

$$\left|R_{ab}\right|^2 = \frac{e^2}{4m_e \omega_{ba}^2}\left(m_e/m_c - 1\right)\left(E_g + \Delta\right)\frac{E_g}{E_g + 2\Delta/3} \qquad (12)$$

where Δ is the spin-orbit splitting in the valence band and *e* is the electron charge. In this perturbation model, the density of electrons *n* is given by:

$$n = \int_{E_g}^{\infty} g_{cvh}(\hbar\omega_{ba})\, f_{ch}(\hbar\omega_{ba})\, d(\hbar\omega_{ba}) \qquad (13)$$

2.2. Numerical calculation of gain coefficients in 1.55 μm InGaAsP lasers

The above theoretical model was applied to calculate the spectral characteristics of the material gain coefficients $g^{(1)}$ and $g^{(3)}$ in $In_xGa_{1-x}As_yP_{1-y}$/InP lasers emitting in wavelength of 1.55 μm. The compositions x and y corresponding to this emission wavelength are 0.93 and 0.436, respectively which correspond to band gap energy of $E_g=0.783$ eV and wavelength $\lambda_g=hc/E_g=1.585$ nm, refractive index $n_r=3.0$, spin-orbit splitting energy of $\Delta=0.321$ eV, and effective masses $m_c=0.0437m_e$, $m_{vh}=0.431m_e$ and $m_{v\ell}=0.058m_e$ with m_e as the electron rest mass [18]. The relaxation times τ_{in}, τ_c and τ_v are assumed equal and set as 0.1 ps. The procedures of calculation of $g^{(1)}$ and $g^{(3)}$ and their dependence on the electron density n were as follows. First the quasi-Fermi levels μ_c and μ_v were determined from the condition of electrical neutrality:

$$\int_{E_g}^{\infty} g_{cvh}(\hbar\omega_{ba})\left[f_{ch}(\hbar\omega_{ba})+f_{vh}(\hbar\omega_{ba})-1\right]+g_{cvh}(\hbar\omega_{ba})\left[f_{v\ell}(\hbar\omega_{ba})-1\right]d(\hbar\omega_{ba})=0 \qquad (14)$$

for pre-specified values of the operating voltage between the junction planes V_{op}, which is related to the difference μ_c-μ_v by

$$V_{op}=\left(\mu_c-\mu_v\right)/e \qquad (15)$$

The calculated values were then used to calculate the density of electrons n via Eq. (13) and the corresponding material gain coefficients via Eqs. (10) and (11). The Simpson's Composite algorithm was applied to calculate the above integrals numerically [19]. The upper limit of the integrals is determined by the photon energy $\hbar\omega_{ba}$ at which the integrand becomes divergent.

Figure 1(a) plots the wavelength ($\lambda=2\pi c/\omega$) profile of the linear gain coefficient $g^{(1)}$ at an injection level of n=1.052x10^{24} m^{-3}. Both the broadening and tail of the linear gain $g^{(1)}$ shown at wavelengths $\lambda<\lambda_g$ come from the intraband relaxation introduced by the Lorenzian spectral distribution that characterizes the gain expression (10). The laser most likely oscillates in the longitudinal mode of wavelength close to the peak wavelength λ_{peak} of the gain profile. The increase in the injected electron density n causes nearly linear increase of the peak value of gain $g_{peak}^{(1)}$, as plotted in Fig. 1(b). By employing these dependencies of $g^{(1)}$ on the photon wavelength λ and the electron density n, $g^{(1)}$ can be approximated with the following simple parabolic function in the vicinity of the gain peak [5]:

$$g^{(1)} = g^{(1)}_{peak}\left(n - n_g - b\left(\lambda - \lambda_{peak}\right)^2\right) \quad (16)$$

Fitting of this expression to the calculated gain is shown in Fig. 1(a). The first term of the above expression counts for amplification of light by stimulated emission, whereas the second term represents the loss by stimulated absorption characterized by the transparency electron density n_g that corresponds to onset of light amplification. The third term contributes to the parabolic dispersion of $g^{(1)}$. Definitions and calculated values of the fitting parameters $g^{(1)}_{peak}$ n_g, and b are given in Table 1. By assuming mode q as the main oscillating mode with a wavelength coinciding with the peak of the linear gain profile ($\lambda_q=\lambda_{peak}$), we calculated the third-order gain coefficient $g^{(3)}$ via Eq. (11). The obtained spectral profile is plotted in Fig. 1(a) on the right and top axes. As the figure shows, $g^{(3)}$ peaks around the central mode $m=q$, but decreases rapidly and symmetrically on both sides of the peak. The peak value of $g^{(3)}$ also changes linearly with n, as shown in Fig. 1(b) on the right axis. Therefore, the third-order gain coefficient $g^{(3)}$ is fitted around the central wavelength by the simple relation [4]:

$$g^{(3)} = \frac{g^{(1)}_{peak}\xi^2 R^2_{cv}\left(n - n_s\right)}{\left(hc/\lambda_m\right)^2\left(\lambda_m - \lambda_n\right)^2 + 1/\tau^2_{in}} \quad (17)$$

Table (1): Definitions and numerical values of fitting parameters characterizing linear and nonlinear gain coefficients in 1.55 μm FP-InGaAsP lasers.

Symbol and definition	Numerical value	Unit
Slope of linear gain with n: $g^{(1)}_{peak}$	9.321×10^{-20}	m^2
Injected electron density at transparency: n_g	8.855×10^{23}	m^{-3}
Injected electron density characterizing nonlinear the gain: n_s	6.746×10^{23}	m^{-3}
Absolute value of the dipole moment: $R_{cv}{}^2$	9.522×10^{-57}	C^2m^2
Dispersion parameter of the linear gain: h	8.173×10^{-5}	$m^{-3}Å^{-2}$

The fittings are displayed in Fig. 1(a) and (b). The calculated values of the fitting parameters n_s and R^2_{cv} are also given in Table 1. By assuming uniform well-designed index guiding structures, the injected electron density n has uniform spatial distribution in the cavity and the transverse modes are limited to the fundamental one [5]. Therefore, the spatial integrations in Eqs. (8) and (9) can be evaluated and the modal gain coefficients are then given as [5]

$$g^{(1)}_m = \xi\, g^{(1)} = g^{(1)}_{peak}\xi\left(n - n_g - b\left(\lambda - \lambda_{peak}\right)^2\right) \quad (18)$$

$$g^{(3)}_{m(m)} = \frac{9}{4V}\xi^2\, g^{(3)} = \frac{9\xi^2}{2V_I}\left(\frac{\tau_{\text{in}}}{\hbar}\right)^2 R^2_{cv} g^{(1)}_{peak}\left(n - n_s\right) \quad (19)$$

$$g_{m(q)}^{(3)} = \frac{3}{2V}\xi^2 g^{(3)} = \frac{4}{3}\frac{g_{m(m)}^{(3)}}{\left(2\pi c\tau_{in}/\lambda_m^2\right)^2\left(\lambda_m-\lambda_q\right)^2+1} \quad (20)$$

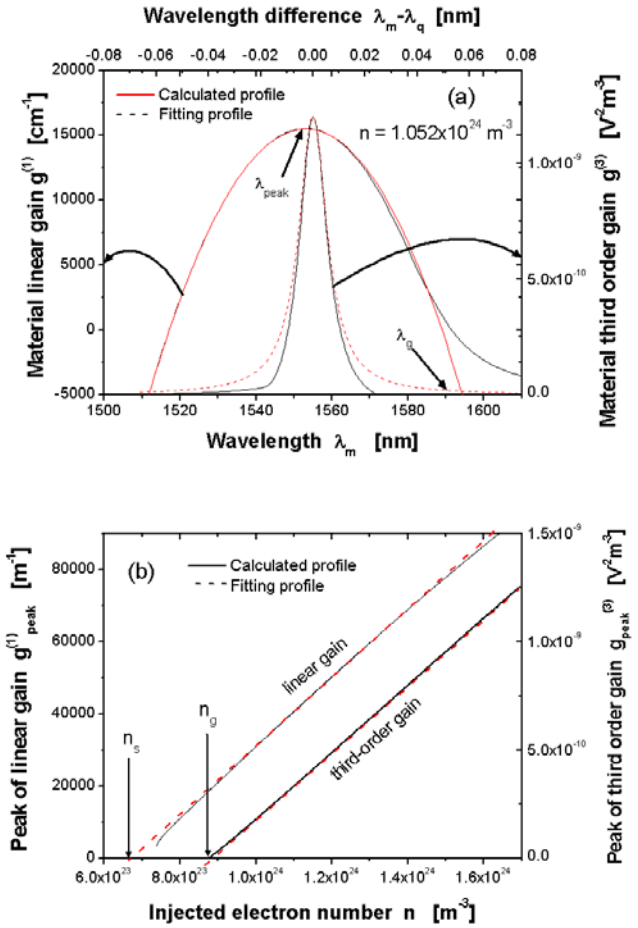

Fig. (1): Characteristics of the material linear gain $g^{(1)}$ and third-order gain $g^{(3)}$: (a) wavelength spectrum when the electron density n=1.052x10^{24} m^{-3}, and (b) variation of the peak values $g_{peak}^{(1)}$ and $g_{peak}^{(3)}$ with n. Fitting of $g^{(1)}$ and $g^{(3)}$ by expressions (16) and (17) are given with dashed lines. Variations of $g_{peak}^{(1)}$ and $g_{peak}^{(3)}$ with n are well fitted with straight lines.

where ξ is the field confinement factor along the transverse vertical direction. The gain is then described by the expression:

$$g_m = g_m^{(1)} - g_{m(m)}^{(3)}\left|\tilde{E}_m\right|^2 - \sum_{q\neq m} g_{m(q)}^{(3)}\left|\tilde{E}_q\right|^2 \quad (21)$$

The second term indicates self-suppression of the gain of mode *m* due to increase in its intensity $\left|\widetilde{E}_m\right|^2$, whereas the third term indicates cross-suppression due to increase in intensity of the other modes $q \neq m$. $g^{(3)}_{m(m)}$ is then called the self-suppression gain coefficient, whereas $g^{(3)}_{m(q)}$ is called the symmetric cross-suppression gain coefficient since it gives similar gain suppressions for wavelength differences of λ_m-λ_q and λ_q-λ_m. It is clear from Eqs. (19) and (20) that $g^{(3)}_{m(q)}$ is larger than $g^{(3)}_{m(m)}$, which then originates in the spatial guiding of the lasing field in the cavity.

In addition to the symmetric type of gain suppression, the oscillating modes exhibit an asymmetric-type of gain suppression. This type originates in vibration of the injected carriers in the beating frequencies of the lasing modes, which adds a new suppressing term to the gain expression. The form of the coefficient of such gain suppression as predicted by Yamada is [10]

$$g^{asym}_{m(q)} = H^{'}_{c} \frac{n - n_g}{\lambda_q - \lambda_m} \tag{22}$$

where the coefficient $H^{'}_{c}$ is a constant depending on the geometry and material parameters of the active region. Equation (22) indicates that the asymmetric gain coefficient $g^{asym}_{m(n)}$ is inversely proportional to λ_q-λ_m and works to suppress the lasing gain for the modes on the short-wavelength side: $g^{asym}_{m(q)} > 0$ for $\lambda_m < \lambda_q$, but works to enhance the lasing gain of the modes on the longer wavelength side: $g^{asym}_{m(q)} <$ for $\lambda_m > \lambda_q$. As equation (22) reads, the effect of $g^{asym}_{m(n)}$ is pronounced at high injection levels. This type of gain suppression may explain the asymmetric gain spectral profile around the main mode observed in experiments [11].

Equation (21) of the suppressed gain is then re-written as:

$$g_m = g^{(1)}_m - g^{(3)}_{m(m)} \left|\widetilde{E}_m\right|^2 - \sum_{q \neq m} \left\{ g^{(3)}_{m(q)} + g^{asym}_{m(q)} \right\} \left|\widetilde{E}_q\right|^2 \tag{23}$$

Calculation of spectra of the suppressed modal gain g_m at a given injection level *I* then requires determination of the intensity of the modal field $\left|\widetilde{E}_m(t)\right|^2$. This task is achieved by simultaneous integration of the rate equations (5) in addition to a rate equation for the injected electron density *n*. This analysis is illustrated in the next section.

3. Multimode Rate Equations of Semiconductor Lasers

It is convenient to change the system of rate equation (5) of the modal field intensity to equations for the modal photon number $S_m(t)$. These physical quantities are interrelated by:

$$S_m(t) = \frac{2\varepsilon_0 n_r^2 \lambda_m}{hc}\left|\widetilde{E}_m(t)\right|^2 \tag{24}$$

which then re-writes Eq. (5) in terms of the electron number $N=nV_I$ as [13]:

$$\frac{dS_m}{dt} = \left(G_m - G_{th}\right)S_m + \frac{a\xi}{V}\left[N - bV\left(\lambda_m - \lambda_{peak}\right)^2\right] \tag{25}$$

where G_m is the gain per unit time of mode m, and is described by the convenient form [12,13]:

$$G_m = \frac{c}{n_I} g_m = A_m - BS_m - \sum_{q\neq m}\left[D_{m(q)} + H_{m(q)}\right]S_n \tag{26}$$

where A_m , B, $D_{m(q)}$ and $H_{m(q)}$ represent the coefficients of linear gain, self-suppression, symmetric cross-suppression and asymmetric cross-suppression, respectively, and are given by:

$$A_m = \frac{c}{n_r} g_m^{(1)} = \frac{a\xi}{V}\left[N - N_g - bV\left(\lambda_m - \lambda_{peak}\right)^2\right] \tag{27}$$

$$B = \frac{c}{n_r} g_{m(m)}^{(3)} = \frac{9}{2}\frac{\pi c}{\varepsilon_o n_r^2 \hbar\lambda_0}\left(\frac{\xi\tau_{in}}{V}\right)^2 a\left|R_{cv}\right|^2\left(N - N_s\right) \tag{28}$$

$$D_{m(q)} = \frac{c}{n_r} g_{m(q)}^{(3)} = \frac{4}{3}\frac{B}{\left(2\pi c\,\tau_{in}/\lambda_q^2\right)^2\left(\lambda_m - \lambda_q\right)^2 + 1} \tag{29}$$

$$H_{m(q)} = \frac{c}{n_r} g_{m(q)}^{asym} = H_c \frac{N - N_g}{\lambda_q - \lambda_m} \tag{30}$$

where

$$a = \frac{c}{n_r} g_{peak}^{(1)} \tag{31}$$

$H_c \approx 3\alpha\lambda_0^2/8\pi c\left(a\xi/V\right)^2$, with α defining the linewidth enhancement factor, is a constant measuring strength of the asymmetric gain $H_{m(q)}$ and will be used

as a parameter to vary $H_{m(q)}$ in this paper. The second term in Eq. (25) represents the rate of coupling of the spontaneous emission into the lasing mode *m*.
Dynamics of the oscillating modes are described by the system (25) of rate equations of $S_m(t)$ combined with the following rate equation of the injected electron number *N* [5]:

$$\frac{dN}{dt} = -\sum_m A_m S_m - \frac{N}{\tau_s} + \frac{I}{e} \ . \tag{32}$$

where τ_s is the electron lifetime due to spontaneous emission. In the present model, we assume that the mode m=0 coincides with the center of the spectral profile of gain, i.e., $\lambda_0 = \lambda_{peak}$. The modes with indices $m>0$ are assumed to lie on the long-wavelength side of the central mode, while the modes with $m<0$ lie on the shorter side. That is,

$$\lambda_m = \lambda_0 + m\Delta\lambda \tag{33}$$

where $\Delta\lambda = \lambda_0^2 / n_r L$, with *L* being the cavity length, is the mode wavelength separation.

4. Simulation of Spectral Profiles of Gain and Laser Output

4.1. Procedures of numerical calculation

The rate equations (25) and (32) of the modal photon number $S_m(t)$ and electron number $N(t)$, respectively, are numerically integrated by means of the fourth-order Runge-Kutta technique. The integration step is set as short as Δt=10 ps, which is short enough to provide fine resolution of the time trajectories of $S_m(t)$. We counted a large number of 15 modes (M=7), i.e., 15 rate equations of $S_m(t)$, in order to gain satisfying insight of the competition phenomena among the oscillating modes. The integration is carried out over a period of T=200 ns. The spectrum of the laser output is calculated in terms of the averaged values $\overline{S}_m$ of the modal photon number over the period *T*. A single-mode oscillation is decided when the photon number ratio of dominant mode to the strongest side mode nearly exceeds 20 dB. The contribution of nonradiative recombination processes, such as Auger recombination, to the lasing process in this long-wavelength laser is introduced in terms of the lifetime τ_s as [20]:

$$1/\tau_s = B_{eff} N \tag{34}$$

where B_{eff} is the effective rate of spontaneous emission by both radiative and non-radiative recombination, and is set as B_{eff}=3.782x10^{-16}/V s^{-1}. The cavity is assumed to have the dimensions of 300μmx5.0μmx0.12μm. The threshold gain level is set as $G_{th}=(c/n_r)g_{th}$=2.72x10^{11} s^{-1} and the confinement factor is ξ=0.2.

4.2. Influence of gain suppression on mode competition and laser output

In this subsection, we illustrate dependence of intensities of the longitudinal modes on the gain suppression effects: namely, self-suppression, symmetric cross-suppression, and asymmetric cross suppression. These analyses are achieved here by comparing the simulation results of the time variations of the modal photon number $S_m(t)$ and the associated output spectra calculated by including and ignoring the corresponding gain coefficients in the rate equations (34). Fig. 2(a)-(h) plots such results when $I=1.6I_{th}$: Fig.2(a) and (b) corresponds to the case of counting the linear gain only (i.e., $B=D_{m(q)},H_{m(q)}=0$), Fig.2(c) and (d) corresponds to the case of ignoring the cross-gain suppression (i.e., $D_{m(q)}=H_{m(q)}=0$), Fig.2(e) and (f) corresponds to ignoring the asymmetric cross-suppression (i.e., $H_{m(q)}=0$), and Fig.2(g) and (h) corresponds to the case of counting all types of gain suppression with $H_c=1.5\text{x}10^{-13}$ ms^{-1}. Figure 2(a), (c), (d) and (e) concerns with time variations of $S_m(t)$, while Fig. 2(e), (f), (g) and (h) concerns with the spectra of the gain G_m and the laser output.

Figure 2(a) shows that after the region of relaxation oscillations, which ends after time less than t=5 ns, the central mode m=0 dominates the instantaneous mode competition. When t=15 ns, the side modes are well suppressed except the modes $m=\pm1$ which still compete with the dominant mode m=0 even when the photon numbers $S_m(t)$ of the modes reach the steady state operation at t=60 ns. Under steady-state operation, the dominant mode carries 73% of the total photon number $\overline{S}$, while each of the modes $m=\pm1$ carries 8.6% of $\overline{S}$, which can be seen in the output spectrum Fig. 2(b). Since the photon number ratio in this case is $\overline{S}_0/\overline{S}_{\pm1}=8.5\text{dB}<20\text{dB}$, the laser is said to oscillate in multi-mode. This multi-mode operation is understood in terms of the gain spectrum shown by the right axis in Fig. 2(b). Although the central mode attains the highest gain approaching the threshold level G_{th}, the gain spectrum is so homogeneous and its suppression is shallow around its center that the neighbor modes $m=\pm1$ have gain $G_{\pm1}$ close to G_0 and then attain high photon numbers $\overline{S}_{\pm1}$.

Fig. 2(c) shows that counting the self-suppression gain, i.e. $B\neq0$, makes the instantaneous mode competition as week as the ratios of the photon numbers of the dominant mode m=0 to the side modes $m=\pm1,\pm2,\pm3$ are not large. The oscillating modes reach the steady-state operation faster in this case: after about 5 ns. This steady-state multi-mode oscillation is indicated also in the output spectrum shown in Fig. 2(d). The homogeneous spectral regime of the gain spectrum shown in Fig. 2(d) becomes wider than the case of Fig. 2(b) promoting the gain of the side modes $m=\pm1,\pm2,\pm3$ which consequently have larger photon numbers.

Influence of the symmetric cross-suppression of gain $D_{m(n)}$, which corresponds to $H_{m(n)}=0$, is illustrated in Fig. 2(e) and (f). Fig. 2(e) shows that the central mode m=0 dominates the mode competition and the laser reaches the steady-state operation as early as $t<12$ ns. The laser output is mostly contained in the central mode indicating a single-mode operation which is confirmed by the output spectrum in Fig. 2(f); $\overline{S}_0 / \overline{S}_{\pm 1} > 30\,\mathrm{dB}$. These results are attributed to the influence of $D_{m(q)}$ to suppress the gain of modes symmetrically on both sides of the central mode with amounts larger than its self-suppression.

It is worth to note that both the gain and output spectra in Fig. 2(b), (d) and (f) are symmetric with respect to the central mode due to the symmetric spectral shape of A_m and $D_{m(q)}$. That is, the photon numbers $\overline{S}_{\pm m}$ with $m\neq 0$ have similar values for the same mode number m. This character is no longer exhibited when the asymmetric cross-suppression of gain $H_{m(q)}$ is included in the modal gain, as shown in Fig. 2(g) and (h). Several features characterize the time variations of the modal photon number $S_m(t)$ shown in Fig. 2(g); (1) the steady-state operation begins after t>25 ns, (2) the mode m=+1 neighbor to the central mode m=0 on the long-wavelength side becomes the dominant mode,(3) the central mode is well suppressed by the instantaneous mode competition after t=10 ns, whereas the mode m=+2 is well suppressed after t=20 ns but is still the strongest side mode, and (4) the modes on the short-wavelength side of the central mode are well suppressed in earlier times. These results are reflected at the output spectrum shown in Fig. 2(h), where the mode m=+1 has the highest photon number $\overline{S}_{+1}$. This photon number exceeds 36 dB of that of the strongest side mode m=+2, indicating single-mode operation. The corresponding gain spectrum shown in Fig. 3(h) is asymmetric showing that the gain of the neighbor modes on the longer side of the central mode m=0 are enhances, while the gain of modes on the shorter side is suppressed. Due to such influence of the asymmetric gain, the gain of mode m=+1 approaches the threshold level G_{th} at expense of the central mode m=0 which then becomes a suppressed side mode.

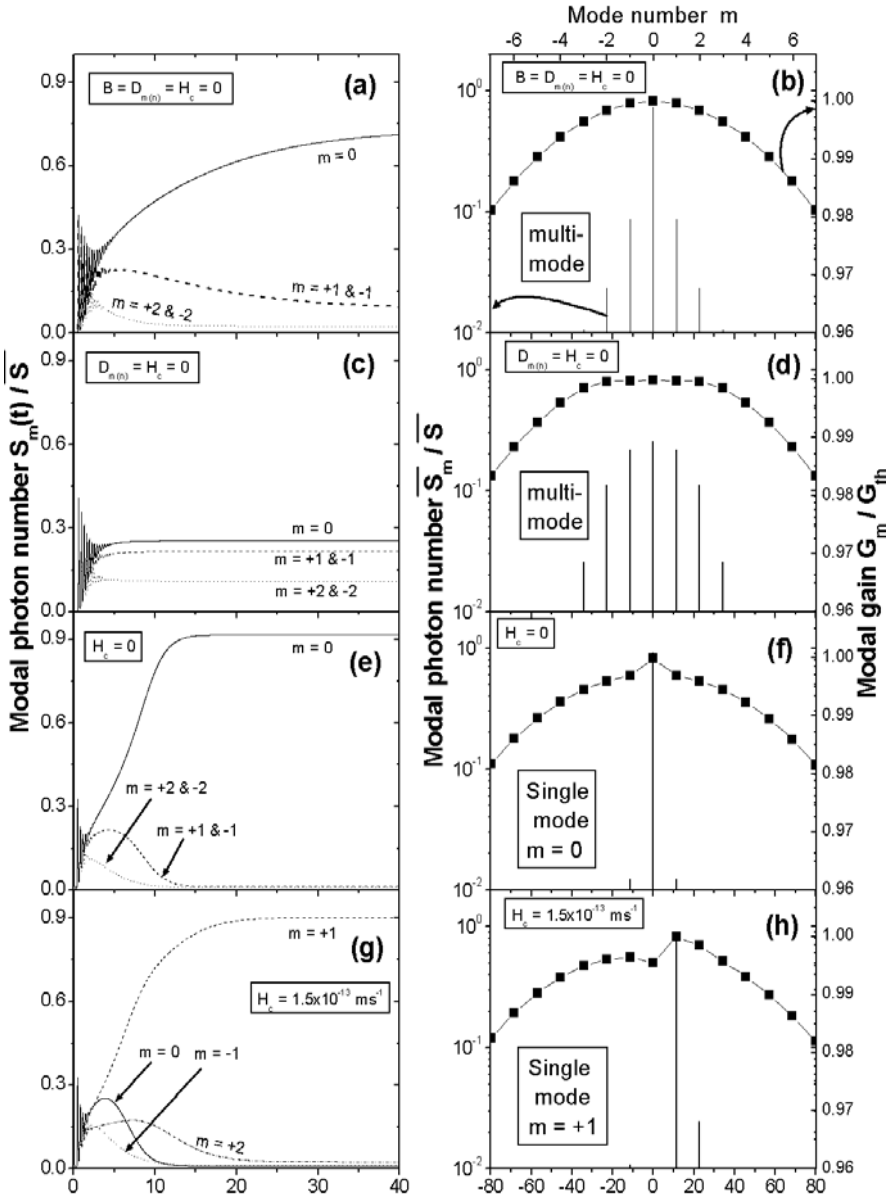

Fig. (2): Simulation results of (a), (c), (e) and (g) time variations of the photon numbers $S_m(t)$ of the most dominant modes, and (b), (d), (f) and (h) the spectra of the laser output and suppressed gain under counting the linear gain only, ignoring the cross-gain suppression, ignoring the asymmetric cross-suppression and counting all types of gain suppression, respectively when $I=1.6I_{th}$. The laser oscillated under a single mode when the cross-suppressions are considered with jumping of the lasing mode to the long-wavelength side when the asymmetric gain suppression is counted.

We extend the above discussion on influence of the gain suppression on the laser output to cover the entire investigated range of injection current: $I=0.9\sim3.0I_{th}$. The results are shown in Fig. 3(a)-(e), which plots the current dependence of the steady-state photon numbers $\overline{S}_m$ of the most dominant modes when $B=D_{m(q)}=H_{m(q)}=0$, $D_{m(q)}=H_{m(q)}=0$, $H_{m(q)}=0$, $H_c=1.5\text{x}10^{-13}$ ms^{-1}, respectively. Under the threshold current I_{th}, the four figures indicate multi-mode operation of the laser. The current range over which the multi-mode operation varies with the type of the gain-suppression included in the rate equations. This multi-mode operation extends over the entire current range: $I=0.9\sim3.0I_{th}$ when $D_{m(q)}=H_{m(q)}=0$. The upper current of this range decreases from $I\sim2.4I_{th}$ when $B=D_{m(q)}=H_{m(q)}=0$ to $I\sim1.44I_{th}$ when $H_c=1.5\text{x}10^{-13}$ ms^{-1} to $I\sim1.36I_{th}$ when $H_c=0$. Except for the case of counting the asymmetric gain suppression, $H_c=1.5\text{x}10^{-13}$ ms^{-1}, the central mode m=0 attains the largest photon number. As Fig. 3(d) shows, inclusion of the asymmetric gain suppression causes jumping of the single-dominant mode from the central one to the neighbor modes on the long-wavelength side m=+1 and +2 when $I=1.4$ and $2.45I_{th}$, respectively. This phenomenon of mode jumping occurring with increase of the current has been observed in experiments [11] and predicted in theory [8-10].

4.2. Influence of asymmetric gain suppression

Interesting features of the laser output are seen when the asymmetric gain suppression is pronounced. The instantaneous mode competition becomes so strong that the modes do not reach steady-state operations; instead several modes on the long-wavelength side of the central mode exhibit instantaneous switching. This is seen in Fig. 4(a), which plots the time variations of the modal photon number $S_m(t)$ when H_c is increased to $3.0\text{x}10^{-13}$ ms^{-1} and $I=2.4I_{th}$. The four modes m=0,+1,+2, +3 and +4 participate in the switching (or hopping) phenomenon. The switching occurs first by the central mode m=0 followed by the other modes in the order of the mode number, and then returns back to the central mode. Such rotation of the lasing mode among the switching modes is repeated regularly. The rotation frequency of the lasing mode as well as the number of switching modes depends on the strength of the asymmetric gain suppression. Such effects can not be simulated when few longitudinal modes are counted in the simulation model. The corresponding spectra of the suppressed gain G_m and the time-averaged photon number are shown in

Fig. 4(b). The figure indicates a hole-burning effect in the vicinity of the central mode of the gain spectrum which exhibits also a high degree of asymmetry. The figure indicates also an asymmetric multi-mode-like output spectrum. These characteristics are in good correspondence with the spectra observed in experiments [3]. Since the characteristics and origins of these multi-mode spectra are different from those dominating the near-threshold regime, this operation is called hopping multi-mode [12].

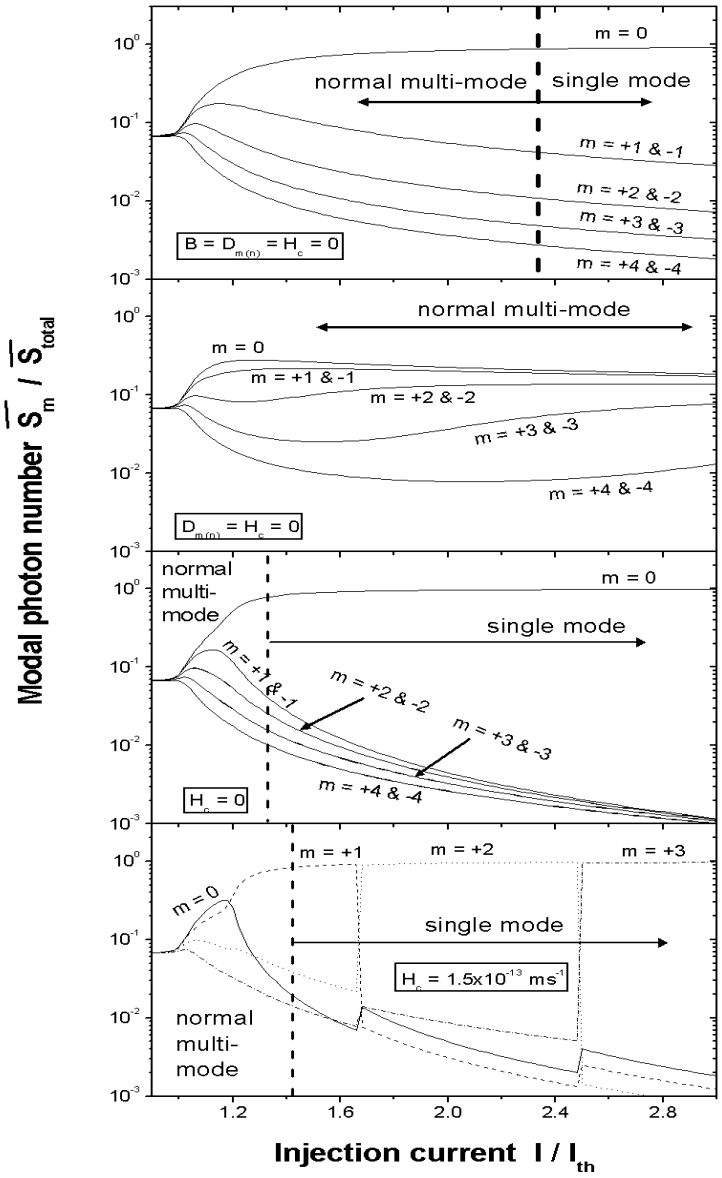

Fig. (3): The time averaged photon numbers $\overline{S}_m$ of the most dominant modes over the current range $I=0.9\sim3.0I_{th}$ when (a) counting the linear gain only, (b) ignoring the cross-gain suppression, (c) ignoring the asymmetric suppression, and (d) counting all types of gain suppressions, respectively. The operation is mostly multi-mode in (a) and (b) when the cross-suppressions are ignored. The laser oscillates in the central mode m=0 under symmetric gain suppression, whereas the lasing mode jumps to modes m=+1, +2 and +3 with increase of I when the asymmetric gain suppression is counted

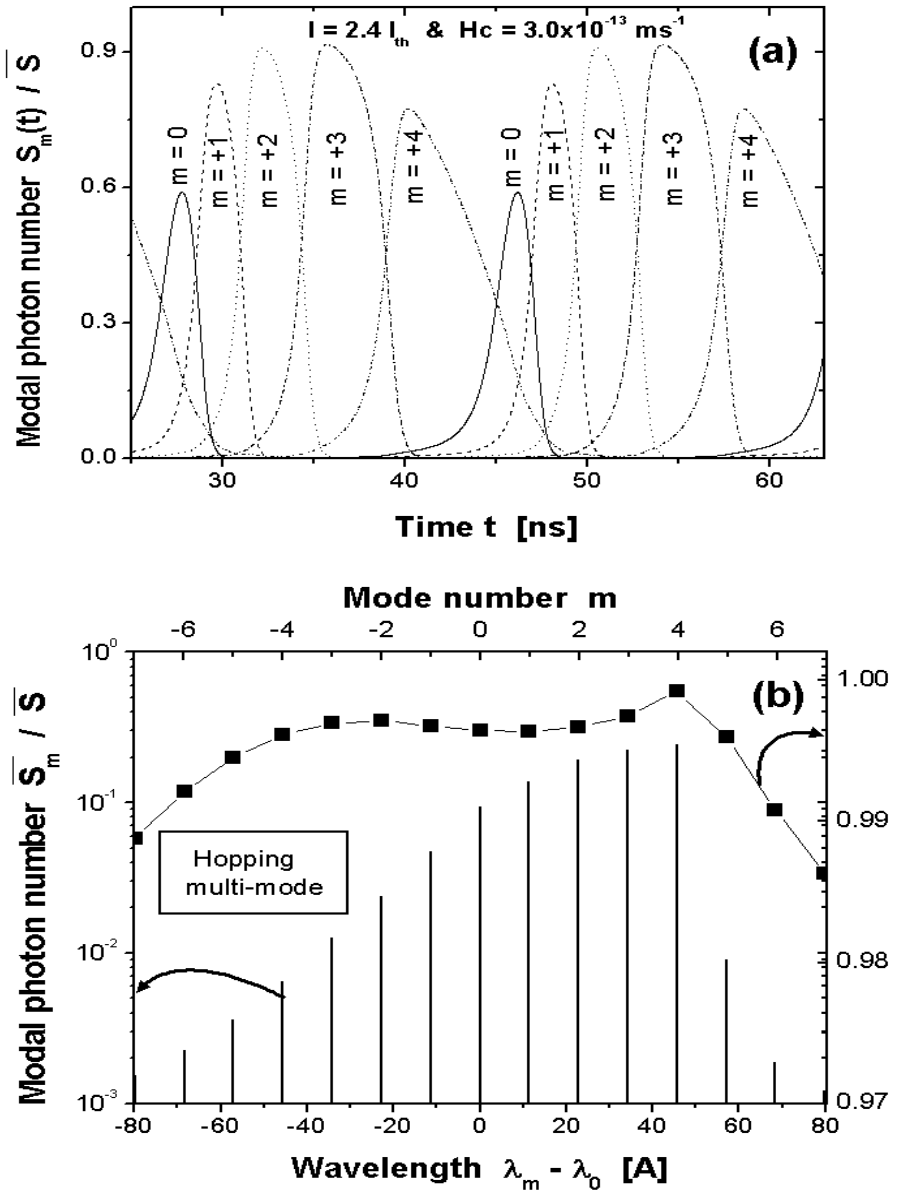

Fig. (4): Characteristics of oscillating modes under strong asymmetric gain suppression: H_c=3.0x10^{-13} ms^{-1} when I=2.4I_{th}: (a) variations of $S_m(t)$ the photon numbers of the most dominant modes m=0, +1, +2, +3, and +4, and (b) the corresponding spectra of the laser output and suppressed gain G_m. Fig. (1) indicates transient switching among the modes, and Fig. (b) indicates strong asymmetry with hole burning in vicinity of the center of the gain spectrum as well as asymmetric output spectrum.

In order to light up the influence of the asymmetric gain suppression on operation of InGaAsP lasers, we did intensive investigations on variations of the time trajectories of the modal photon numbers $S_m(t)$ with strength of the asymmetric gain suppression H_c over wide range of current $I = 0.9 \sim 3.0 I_{th}$. The results were used to plot the (I-H_c) diagram of laser operation shown in Fig. (5). The lower limit, $H_c=0$, corresponds to symmetric gain suppression. The figure indicates many typical features of dependence of laser operation on the asymmetric gain suppression and current: (1) the laser operates in normal multi-mode when injected little above the threshold current I_{th} at injection current I near the threshold *(up to* $I>1.35I_{th}$*)* over the entire range of H_c, (2) the single mode oscillation dominates for operation with small and moderate values of H_c, (3) the increase in H_c causes shift of the lasing mode towards the long-wavelength side and entrance to region of hopping multi-mode operation, (4) the laser operation is dominated with the hopping multi-mode operation when the asymmetric gain suppression is enhanced. Enhancement of the asymmetric gain suppression $H_{m(n)}$ is achieved either by moderate values of H_c associated with high injection current I (example is H_c=2.25x10^{-13} ms^{-1} *and* $I>2.46I_{th}$) or large values of H_c (example is H_c>3.75x10^{-13} ms^{-1}), as indicated by Eq. (30). The operation with moderate values of H_c may correspond to InGaAsP lasers with quantum-well structures, while the large values of H_c may characterize lasers with conventional cavities [21].

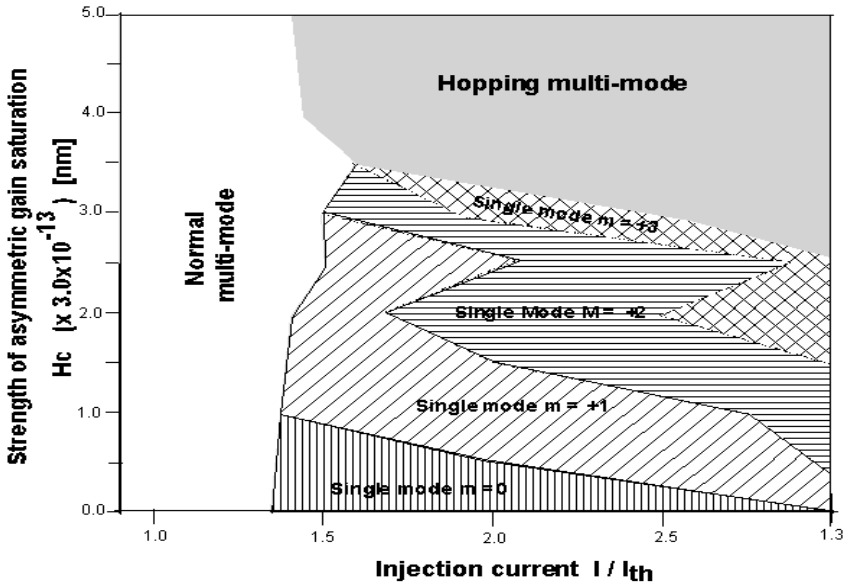

Fig. (5): Schematic map (I-H_c) of operation of 1.55 μm InGaAsP lasers. The lower limit, $H_c=0$, corresponds to symmetric gain suppression. The laser operates in normal multi-mode when injected little above I_{th}. *(up to* $I>1.35I_{th}$*)*. The single mode oscillation dominates for operation with small and moderate values of H_c. The increase in H_c causes jumping of the lasing mode towards the long-wavelength side. The laser operates in hopping multi-mode under

high H_c.

5. Conclusions:

We presented intensive investigations of influences of the nonlinear gain suppression on the mode intensities and modal operation in 1.55 μm InGaAsP lasers. Both self- and cross-suppression effects of modal gain were characterized. We introduced a schematic map of laser operation over wide ranges of the strength of the asymmetric gain suppression and injection current. The obtained results indicated that:

(1) The laser oscillates in multi-modes if injected near the threshold level.
(2) The self-gain suppression induces multi-mode operation, whereas the symmetric cross-suppression induces operation only in the central mode of the gain spectrum.
(3) Weak or moderate asymmetric gain suppression causes single-mode operation with the lasing mode jumping to the long-wavelength side of the central mode

Strong asymmetric gain induces transient switching among several modes on the long-wavelength side of the gain spectrum resulting in asymmetric output spectra.

References:

1. J. Buus, *Single frequency semiconductor lasers*, Bellingham, WA: SPIE Optical Engineering Press, Chap. (2) (1991).
2. T. P. Lee, C. A. Burrus, J. A. Copeland, A. G. Dentai, and D. Marcuse, *IEEE J. Quantum Electron.*, vol. **QE-18**, 1101, (1982).
3. I. Mito, M. Kitamura, K. Kaede, Y. Odagiri, M. Seki, M. Sugimoto, K. Kobayashi, *Electron. Lett.*, **18**, 2, (1982).
4. J. Manning, R. Olshansky, D. M. Fye, and W. Powazinik, *Electron Lett.*, **12**, 496, (1985).
5. M. Yamada and Y. Suematsu, *J. Appl. Phys.*, **52**, 2653, (1981).
6. G. P. Agrawal, IEEE J. Quantum Electron. **QE- 23**, 860 (1987).
7. M. Ahmed and M. Yamada, SPIE, **3283**, 485, (1999).
8. H. Ishikawa, M. Yano, and M. Takusagawa, *Appl. Phys. Lett.,* **40**, 553, (1982).
9. Ogasawara and R. Ito, *Jpn. J. Appl. Phys.*, **27**, 615, (1988).
10. M. Yamada, *J. Appl. Phys.*, **66**, 81, (1989).
11. N. Ogasawara and R. Ito, *Jpn. J. Appl. Phys.*, **27**, 607, (1988).
12. M. Ahmed and M. Yamada, IEEE J. Quantum Electron., **38**, (6), 682, (2002).
13. M. Ahmed, *Phys. D.*, **176**,. 212, (2003).

14. M. Yamada, *IEEE J. Quantum Electron.*, **QE-22**, 1052, (1986).
15. M. Ahmed and M. Yamada, *J. Appl. Phys*., **84**, (6), 3004, (1998).
16. C. H. Gooch, "*Gallium Arsenide Lasers"*, Wiley-Interscience, New York, 36, (1969).
17. Y. Suematsu and A. R. Adams, *Hand Book of Semiconductor Lasers and Photonic Integrated Circuits*, London: Chapman and Hall, chapt 4, (1994).
18. G. P. Agrawal and N. K. Dutta, *Semiconductor lasers*, New York: Van Nostrand Reinhold (1993).
19. R. L. Burden, J. D. Faires and A. C. Reynolds, "Numerical Analysis", 2nd Ed., (Prindle, Weber and Schmidt, Boston (1981).
20. S. Ogita, A. J. Lowery, and R. S. Tucker, *IEEE J. Quantum Electron.*, **QE-33**, 198 (1997).
21. T. Higahsi, T. Yamamoto, S. Ogita and M. Kobayashi, IEEE J. Selected Topics in Quantum Electron., **3**, (2), 513 (1997).